Engineering Reports

WILEY

Engineering Reports Open Access

RESEARCH ARTICLE OPEN ACCESS

Accumulated Performance Comparison of Solar PV and Solar Thermal Water Heating in New Zealand

Wei Lu[1,2] | Jay Wang[1]

[1]School of Engineering, Computer & Mathematical Sciences, Auckland University of Technology (AUT), Auckland, New Zealand | [2]Guangdong Provincial Mechanical Engineering Experimental Teaching Center, Guangdong Technology College, Zhaoqing, China

Correspondence: Jay Wang (jay.wang@aut.ac.nz)

Received: 29 July 2025 | **Revised:** 28 September 2025 | **Accepted:** 23 November 2025

Keywords: accumulated performance | solar PV system | solar thermal system | water heating systems

ABSTRACT

The rising global energy demand and environmental harm caused by reliance on fossil fuels highlight the urgent need for sustainable solutions in residential water heating. This study conducts a comparative numerical analysis of solar photovoltaic (PV) and solar thermal water heaters under New Zealand's typical weather conditions. By integrating the National Institute of Water and Atmospheric Research (NIWA) meteorological data, hourly simulation results were performed to analyze energy output, water temperature profiles inside storage tank, and levelized cost of electricity (LCOE) under varying seasonal conditions, including summer, normal, and winter. The highlight of this study is the evaluation of accumulated water performance within the storage tank under real-life operating conditions. This includes the impact of actual weather fluctuations (including ambient temperature and solar radiation), target hot water temperature, heat losses from the tank, and typical household water usage patterns along with the replenishment of cold water. Under identical weather conditions, the simulations results indicate that the solar thermal system outperforms solar PV system across key performance metrics. For solar water heating applications, the thermal system generated 5847.59 kWh of energy annually per 10 m^2 of collector area, compared to 2780.41 kWh from the PV system. Although the thermal system required 33.7% more auxiliary energy annually (964.59 kWh) compared to the PV system (721.38 kWh), it delivered better energy utilization efficiency. This is highlighted by its produced-to-used energy ratio of 6.06, which is 58% higher than the PV system's ratio of 3.85. The efficiency translated to better economic advantages, with thermal achieving a 61.9% lower LCOE for produced energy at 0.0766 NZD/kWh compared to PV's 0.2013 NZD/kWh, and a 40.2% lower LCOE for used energy at 0.4641 NZD/kWh versus PV's 0.7757 NZD/kWh.

1 | Introduction

The rapid growth of the global population is directly driving a corresponding increase in energy demand, while the continued reliance on fossil fuel-based energy systems remains a major contributor to environmental degradation, posing a significant global challenge [1]. Household water heating accounts for a significant proportion of residential energy use in New Zealand, representing 26% of total household electricity consumption, with electric hot water cylinders predominantly used, installed in more than 85% of dwellings [2]. In fact, solar energy is a clean and renewable resource that enables effective fulfillment of domestic water heating demands via two main approaches [3]: (1) direct solar-thermal conversion [4, 5], which transforms incident

Abbreviations: COP, coefficient of performance; LCOE, levelized cost of electricity (NZD/kWh); NIWA, National Institute of Water and Atmospheric Research; NOCT, nominal operating cell temperature (°C).

radiation into thermal energy, and (2) photovoltaic (PV)-electric systems [6], where the generated electricity is used to operate auxiliary heating devices. Both technological methods ensure consistent thermal delivery for domestic applications while substantially mitigating the environmental footprint associated with conventional water heating methods [7].

Within the unique temperate marine climatic regime of New Zealand [8], solar thermal and PV heating systems demonstrate disparities in operational concepts and performance metrics. Solar thermal technology leverages collector units to directly transform solar irradiance into thermal energy, achieving heat conversion efficiencies up to 75% [9]. In contrast, PV-based heating systems substantially constrained practical thermal efficiencies confined to the 7%–16% range due to cascading energy losses inherent in the sequential PV conversion and resistive heating processes [10]. Despite pronounced seasonal irradiance variability enabling PV heating systems to supply 29%–47% of annual residential electricity consumption within cogeneration-integrated hybrid energy frameworks [10], their high upfront costs and comparatively low thermal efficiency of PV heating systems continue to hinder their full replacement of solar thermal systems within New Zealand's residential sector.

Numerous investigations have employed simulation methods to evaluate the thermal behavior of solar water heating systems. Halawa and his colleagues comprehensively examined thermal performance rating methodologies for solar water heating installations across Australia, Taiwan, Japan, and other regions, establishing that sophisticated rating frameworks prove more effective for energy conservation and greenhouse gas mitigation [11]. In China, Xu et al. engineered an active solar water wall system incorporating hollow polycarbonate panel structures, which demonstrated satisfactory solar thermal harvesting and release capabilities [12]. In New Zealand, Bishop investigated intelligent control systems for electric hot water cylinders, implementing peak electricity load shifting that substantially enhanced demand-side management performance [13].

Concurrently, the application of advanced computational intelligence techniques, such as machine learning and nature-inspired optimization algorithms, has emerged as a powerful trend in solar energy system design and analysis. Recent studies have demonstrated their efficacy in enhancing model accuracy and solving complex optimization problems. For instance, Long short-term memory networks combined with the brown-bear optimization algorithm have been successfully applied to model floating solar power systems [14]. Similarly, seasonal dynamic modeling assisted by machine learning (ML), and multi-objective genetic optimization has been employed for the comprehensive energy and economic analysis of building-integrated photovoltaic thermal systems [15]. Beyond heating applications, exergoeconomic and environmental assessments integrating these advanced methods are also being applied to evaluate solar-driven cooling and ventilation systems [16]. These advancements underscore a paradigm shift towards data-driven, high-fidelity modeling approaches in renewable energy research.

Despite these advancements, extensive studies dedicated to the single daily performance optimization of solar water heating systems, aim to enhance their overall efficiency and operational performance. These investigations typically employ parametric approaches examining material properties and structural configurations to characterize single-day system performance. However, such studies exhibit a fundamental methodological limitation through their neglect of accumulated performance evaluation under real weather conditions, actual water consumption during the day, and heat losses from the tank, for both solar thermal and solar PV water heating systems.

To address this research gap, the present study conducts a systematic comparative analysis of solar PV and solar thermal water heaters through numerical analysis across consecutive operational cycles under real weather conditions. This study employs a streamlined system modeling approach integrated with the National Institute of Water and Atmospheric Research (NIWA) climate data to address key challenges in predicting the accumulated system performance of solar water heating systems. The primary research objectives include:

1. To create mathematical models of storage tanks integrated with solar PV hot water systems and solar thermal water heater systems, with the goals of precisely quantifying the temperature and energy variations in solar water heaters arising from the water demand patterns in the Auckland region.
2. To employ the developed numerical models to conduct system performance simulations using typical meteorological year data, covering three representative weeks: one in summer, one in winter, and one in the intermittent season.
3. To evaluate the total annual electricity generation and the corresponding average electricity cost for two system configurations, and to perform a levelized cost of electricity (LCOE) analysis to compare their long-term economic performance.

2 | System Configurations

The solar PV water heater system, as illustrated in Figure 1a, mainly comprises solar PV modules (including solar PV devices and an inverter), a water storage tank, an electric heater, a controller, water delivery ports (cold and hot), and valves. The system integrates solar PV modules with a water heating setup to efficiently supply hot water to end users. Solar PV modules capture solar radiation and convert it into electrical energy, which is managed by a controller to regulate power delivery to the heater located inside the water storage tank. Cold tap water enters the tank through an inlet valve at the bottom, and the heater, typically a resistive coil, uses the PV-generated electricity to heat the water stored in the tank. Once heated, the water is supplied to end users through the outlet valve at the top of the tank as needed. The controller continuously monitors the system's status and water temperature to ensure safe and efficient operation while preventing overheating or unnecessary energy consumption.

The system shown in Figure 1b integrates a solar thermal collector with a water heating and storage system for domestic hot water supply. Solar radiation is absorbed by the solar collector, which heats the water circulating through it. Cold tap water

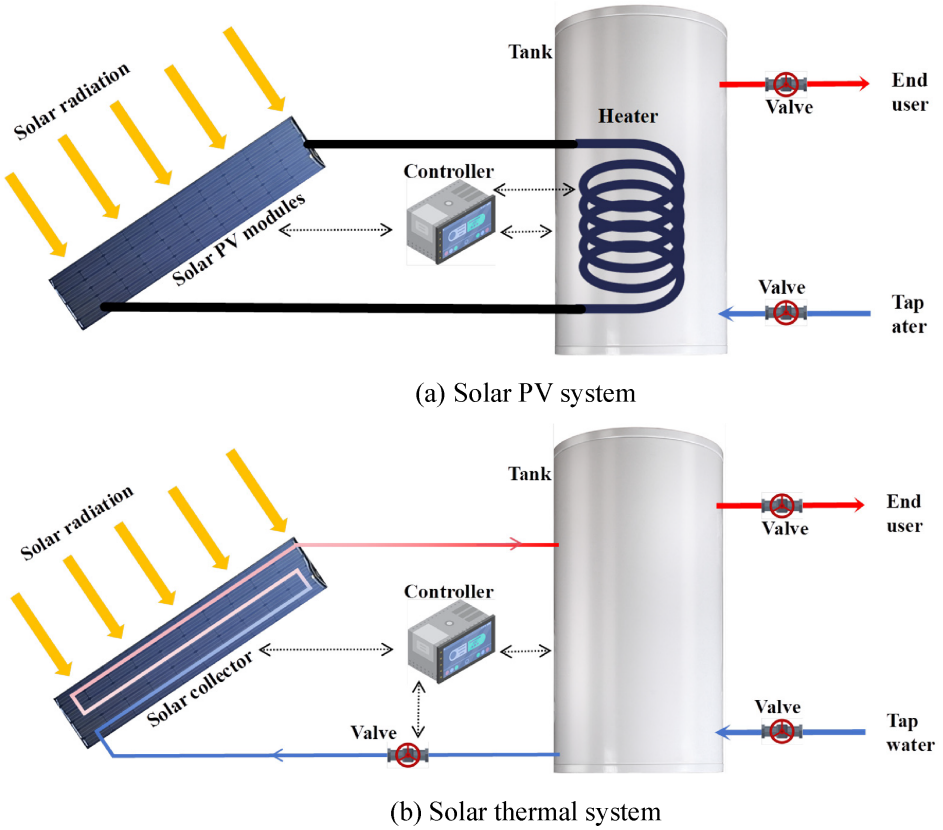

FIGURE 1 | Schematic diagrams of solar water heating systems.

enters the system through an inlet valve, and a controller manages the operation of pumps and valves to circulate water between the solar collector and the storage tank, ensuring efficient heat transfer. Heated water from the solar collector flows into the storage tank, where it is stored until needed by the end user. Hot water is then supplied from the tank to the end user through an outlet valve when there is demand. The controller continuously monitors system parameters to optimize heat collection and ensure safe operation, preventing overheating and managing the flow of water within the system.

3 | Numerical Model and Control Strategy

This study will numerically analyze the accumulated performance of the solar PV and solar thermal water heating system under real climatic conditions for a consecutive period of time. Key assumptions for this numerical model have been made, including: (1) Solar radiation is assumed uniform over the solar collector and solar PV surface, and shading effects are neglected. (2) Systems are assumed to operate under steady-state conditions for hourly or daily simulation intervals. (3) Thermal losses from the tank and pipes are assumed to be within standard values or are neglected. (4) Controllers function seamlessly, ensuring optimal switching for pumps and load management without delays.

3.1 | Solar Thermal Heating

In solar thermal modeling, Reynolds number (Re) is used to calculate the ratio of inertial forces to viscous forces, while the Prandtl number (Pr) characterizes the relationship between momentum diffusivity and thermal diffusivity in a fluid. They can be determined from [17]:

$$Re = \frac{\rho \mu D}{\lambda} \tag{1}$$

$$Pr = \frac{uC_p}{k_{\text{fluid}}} \tag{2}$$

where μ is water fluid speed, ρ is water density, D is tube diameter, λ is water viscosity, u is the dynamic viscosity of water, C_p is the specific heat of water, and k is the thermal conductivity of water.

Under the conditions of $2300 < Re < 5 \times 10^6$ and $0.6 \leq Pr \leq 10^5$, Nusselt number (Nu) for the laminar flow can be determined from [18]:

$$Nu = \frac{\left(\frac{f}{8}\right)(Re - 1000)Pr}{1 + 12.7\left(\frac{f}{8}\right)^{\frac{1}{2}}\left(Pr^{\frac{2}{3}} - 1\right)} \tag{3}$$

where f is the friction factor, which can be calculated from [19]:

$$f = \frac{1}{(1.82 \ln Re - 1.64)^2} \tag{4}$$

Heat transfer coefficient (h_{fi}) between the fluid and the tube wall can be determined from [18]:

$$h_{\text{fi}} = \frac{\text{Nuk}_{\text{filud}}}{D} \tag{5}$$

The standard fin efficiency (F) for straight fins with rectangular profile and the fin parameter (m) can be calculated [20]:

$$F = \frac{\tan h\left[\frac{m(W-D)}{2}\right]}{\frac{m(W-D)}{2}} \tag{6}$$

$$m = \sqrt{\frac{U_L}{k_{\text{plate}}\delta}} \tag{7}$$

where W is the distance between the tubes, k_{plate} is the thermal conductivity of plate, U_L is the overall heat loss coefficient and δ is absorber plate thickness.

The collector efficiency factor (F') can be determined from [20]:

$$F' = \frac{\frac{1}{U_L}}{W\left[\frac{1}{U_L+[D+(W-D)F]} + \frac{1}{C_b} + \frac{1}{\pi D_i \mathrm{h}_{fi}}\right]} \tag{8}$$

where D_i is the inside tube diameter, and C_b is the bond conductance.

The collector heat removal factor (F_r) can be determined from [21]:

$$F_r = \frac{\dot{m}C_p}{U_L A_c}\left(1 - e^{\frac{-F'U_L A_c}{\dot{m}C_p}}\right) \tag{9}$$

where $\dot{m}$ is the mass flow rate and A_c is the solar collector area.

The product of solar irradiance on the tilted surface (G_t) is calculated as [10]:

$$G_t = G\ \cos\theta \tag{10}$$

where G, *is* a horizontal surface and θ is the tilt angle of the PV modules.

The rate of useful energy gain (Q_u) for solar thermal water heaters is determined from [22]:

$$Q_u = A_c F_r\left[G_t\ (\tau_a) - U_L(T_i - T_a)\right] \tag{11}$$

where τ_a is the transmittance-absorptance product, T_i is the inlet water temperature, and T_a is the ambient air temperature.

3.2 | Solar PV Heating

In solar PV model, the daily net PV power output (Q_{out}) is calculated from [23]:

$$Q_{\text{out}} = \int_0^a G_t A \eta_{\text{PV}} \eta_{\text{inv}} dt \tag{12}$$

where η_{PV} is PV system efficiency, η_{inv} is inverter efficiency, A is panel area, and a is time.

The PV temperature (T_{PV}) is calculated from [24]:

$$T_{\text{PV}} = T_a + (\text{NOCT} - T_{a,\text{ref}})\frac{G_t}{G_{t,\text{ref}}} \tag{13}$$

where T_a is the ambient temperature and NOCT is the nominal operating cell temperature provided by the manufacturer, measured at a reference solar irradiance $(G_{t,\text{ref}})$ and a reference ambient temperature $(T_{a,\text{ref}})$.

3.3 | Water Storage Tank

In the water storage tank, the water temperature after usage (T_{use}) can be calculated from:

$$T_{\text{use}} = \frac{(M - m_{\text{use}})T_{f,i-1} + m_{\text{use}}T_{\text{cold}}}{M} \tag{14}$$

where M is the total mass of water inside the tank, m_{use} is the amount of water mass used, $T_{f,i-1}$ is the water temperature at the previous hour, and T_{cold} is the water temperature at the tank inlet.

The energy loss for the water temperature (Q_{loss}) can be calculated from [25]:

$$Q_{\text{loss}} = U_{\text{tank}} A_{\text{tank}}(T_{\text{use}} - T_a) \tag{15}$$

where U_{tank} is the heat loss coefficient of tank and A_{tank} is the surface area of tank.

The final water temperature of the current hour (T_f) can be calculated from:

$$T_f = T_{\text{use}} + \frac{(q_i - Q_{\text{loss}})}{MC_p} \tag{16}$$

where q_i is the hourly input energy.

3.4 | System Performance

The coefficient of performance (COP) is defined as the ratio of the usable thermal energy delivered by the solar water system to the total available solar energy input, which can be expressed as [26]:

$$\text{COP} = \frac{Q_{\text{eff}}}{Q_{\text{all}}} \tag{17}$$

where Q_{eff} is the total usable thermal energy delivered to water heating and Q_{all} is the total solar energy from the solar radiation.

The levelized cost of electricity (LCOE) is calculated from [27]:

$$\text{LCOE} = \frac{\sum_{t=0}^{T}(I_t + O_t + D_t)/(1+r)^t}{\sum_{t=0}^{T} S/(1+r)^t} \tag{18}$$

where T is project lifetime, t is year index, I_t is investment cost, O_t is operational costs, D_t is decommissioning value, r is country-specific discount rate, and S is rated annual energy output.

3.5 | Control Logics

The control algorithm of the simulation model for solar water heaters has been illustrated in Figure 2. The process begins by entering parameters, such as tank volume V_{tank}, water mass flow rate $\dot{m}$, specific heat capacity C_p, tank surface area A_{tank}, water usage mass m_{use}, and so forth. The weather data will be firstly read, and the data including solar irradiance (G) and ambient temperature (T_a), which will influence the heating process and heat loss inside the tank. The model will check if there is water usage at the current time. If so, it calculates the mass of water used (m_{use}) and the stabilized temperature after usage (T_{use}). The model computes the accumulated energy within the hour by considering the energy input (e.g., hourly solar radiation, q_i) and energy losses (e.g., heat loss to the environment, Q_{loss}). Using the energy balance, the model calculates the hourly temperature change (ΔT) and updates the final temperature (T_f). The process checks if the final temperature of water exceeds the maximum allowable temperature required (T_{max}). If $T_f \geq T_{max}$, the heating process is stopped, and the temperature is bounded by T_{max}. Otherwise, the heating process continues. The system moves to the next time point and repeats the process. The loop continues until a week has passed. Once completed, the system outputs a performance curve (including temperature trends or efficiency metrics) and ends.

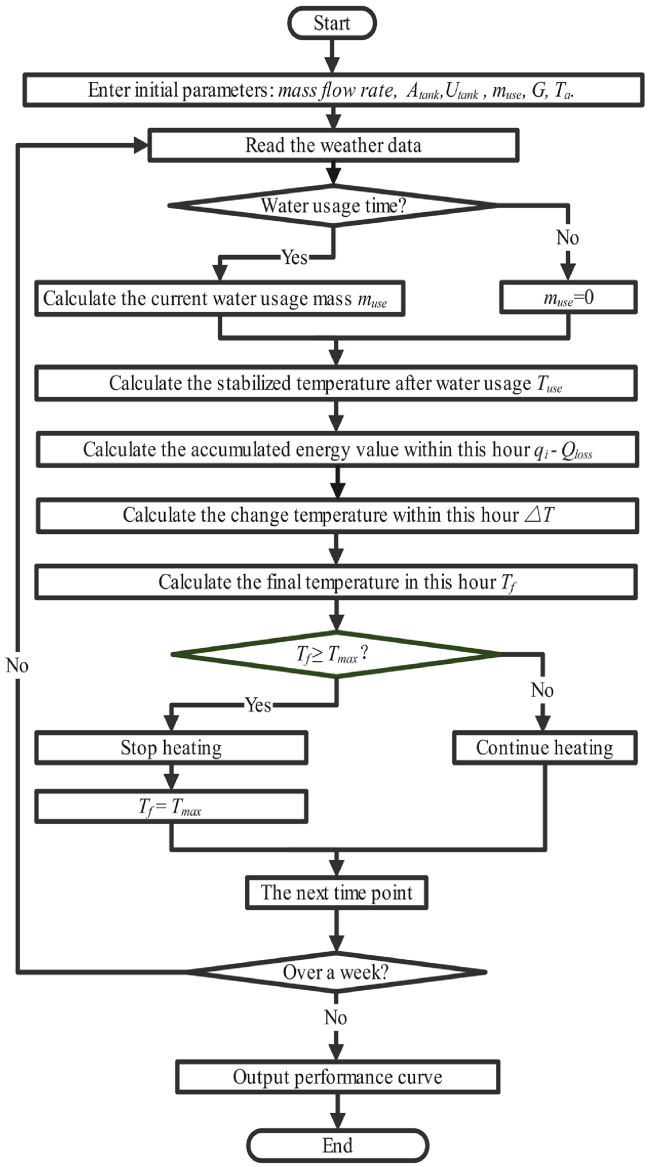

FIGURE 2 | Control system diagram.

4 | Case Study

4.1 | Initial Operating Conditions

Hourly meteorological data (including ambient temperature, solar radiation, and sunshine hours) used in this numerical analysis were sourced from the NIWA, New Zealand [28]. The specific weather data used were obtained from Auckland North Shore Albany Environmental Monitoring Station (Agent Number: 37852). It can be assumed that when the hot water is consumed, an equivalent volume of cold water is immediately replenished into the storage tank. During the summer season (December to February), the cold-water temperature is set at 25°C, with a target hot water outlet temperature of 45°C and the transmittance-absorptance ($\tau\alpha$) is 0.75. In winter (June to August), the cold-water temperature is lowered to 15°C, with a target hot water outlet temperature of approximately 55°C, and $\tau\alpha$ is 0.8. Under normal weather conditions (March to May and September to November), the cold-water temperature is maintained at 20°C, the target hot water outlet temperature is 50°C, and the $\tau\alpha$ is 0.775. The initial conditions inside the water storage tank have been illustrated in Table 1. The key design parameters for both solar PV hot water systems and solar thermal water heater systems are summarized in Table 2.

In the sensitivity analysis, the effect of mass flow rate ($\dot{m}$) on the heat removal factor (F_r) of the solar systems was examined. To do this, the mass flow rate was varied from 0.01 to 0.20 kg/s in uniform increments of 0.001 kg/s, as illustrated in Figure 3. This range represents typical operating conditions and ensures that the analysis systematically captures how changes in flow rate influence the key output variables.

This study employs a mass flow rate of 0.08 kg/s, determined through a comprehensive balance between heat transfer performance and system energy consumption. This flow rate ensures

TABLE 1 | Initial parameters for the water storage tank.

Parameter	Value
Total water volume in the tank V_{tank}	200 L
Daily hot water usage schedule	9 am (50 L), 1 pm (50 L), and 7 pm (50 L)
Water mass flow rate $\dot{m}$	0.08 kg/s
Water specific heat C_p	4180 J/kg·K
Water density	988 kg/m^3
Surface area of tank A_{tank}	1.5 m^2
Heat loss coefficient of tank U_{tank}	1.5 W/m^{2}K

TABLE 2 | Key design parameters for the solar-PV and solar-thermal systems.

Parameter	Value
Tube distance W	0.12 m
Outer tube diameter D	0.01 m
Inner tube diameter D_i	0.008 m
Solar collector area A_c	10 m^2
Solar PV area A	10 m^2
Absorber plate thickness δ	0.0005 m
Plate thermal conductivity k_{plate}	200 W/m·K
Water thermal conductivity k_{fluid}	0.640 W/m·K
Overall heat loss coefficient U_L	5 W/m^2·K
Bond conductance C_b	300 W/m·K
Tilt θ	19°
NOCT	45°C
PV system efficiency η_{PV}	0.2
Inverter efficiency η_{inv}	0.97
Dynamic viscosity u	1.002×10^{-3} Pa·s
Absorber plate thickness δ	0.0005 m

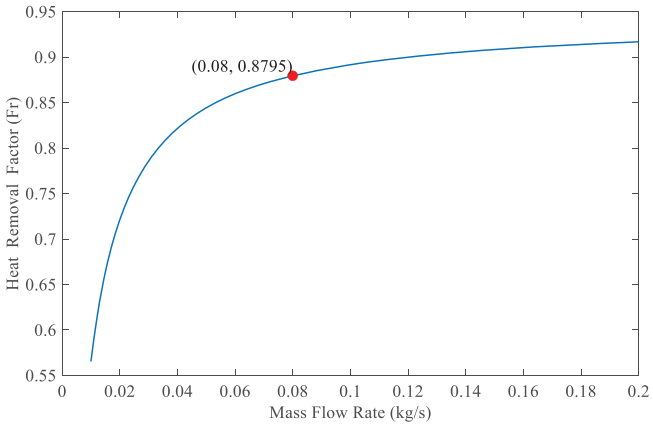

FIGURE 3 | Sensitivity analysis.

the fluid operates within a fully turbulent flow regime, significantly enhancing the heat transfer coefficient via intensified boundary layer disturbance. Simultaneously, it avoids the sharp increase in pressure drop and excessive pumping power consumption associated with higher flow rates. While meeting target thermal load and temperature rise constraints, this design achieves an optimal integration of enhanced heat transfer efficiency and operational economy. It offers a practical level of operational redundancy for the system, reflecting a balanced design approach that combines engineering feasibility with energy efficiency optimization.

4.2 | Performance Analysis

This section compares the performance of Solar-PV and Solar-Thermal systems over a seven-day period across three typical seasons in New Zealand: summer, winter, and an intermediate season (characterized by normal weather conditions). The summer dataset covers the period from 8 to 14, December 2020. The normal season dataset covers the period from 12 to 18, April 2020. The winter data set covers the period from 3 to 9, July 2020. Figure 4a,b indicate the seven-day temperature and solar irradiance profiles recorded at the Albany monitoring station, located in North Shore, Auckland, NZ. The graphical analysis reveals that both temperature and solar irradiance peak during summer conditions, followed by normal weather patterns, with winter exhibiting the lowest measurements.

4.2.1 | Accumulated Hourly Temperature Profiles

Figure 5a presents the seven-day continuous water temperature in the PV system's storage tank under three typical weather conditions. The PV-based water heating system shows moderate temperature stability in summer, with the storage tank fluctuating between 37°C and 45°C. During the day, the tank heats up gradually, but experiences temperature drops during water usage, especially under low sunlight conditions. Under normal weather conditions, the system shows increased variability, with the water temperatures ranging from 30°C to 50°C and more noticeable drops after draw-off events, reflecting a dependence on real-time solar availability. In winter, performance declines significantly, with tank temperatures falling to between 19°C and 37°C. The system struggles to recover after usage, resulting in inconsistent hot water supply during colder and low-irradiance periods.

Figure 5b illustrates the seven-day continuous water temperature in the solar thermal system's storage tank under three typical weather conditions. In summer, the tank temperature varies stably, with a pattern of steady daytime heating followed by sharp drops during draw-off events. The thermal system's storage tank maintains stable water temperatures (36°C–45°C) during summer operation, exhibiting rapid thermal recovery following temperature decrease caused by draw-off events at 09:00 and 13:00, respectively. Under nominal meteorological conditions, the system demonstrates equivalent recovery efficiency to achieve the water temperature (31°C–50°C), promptly compensating for temperature declines after 11:00 draw-off events. During winter operation, it sustains baseline heating capacity, maintaining operation across wider temperature bands (21°C–49°C) despite low-irradiance conditions. All seasons collectively demonstrate rapid thermal recovery characteristics, ensuring consistent and stable hot water supply.

In comparing both systems, the solar thermal system maintains more stable and higher water temperatures than the PV system across all weather conditions. On normal days, both solar PV and thermal systems reach similar peak temperatures (50°C), but the solar thermal system sustains these temperatures for a longer duration and recovers faster after water draw-offs. The solar thermal system performs better in winter, maintaining higher baseline temperatures (21°C–49°C) compared to the PV system (19°C–37°C), which struggles to recover after usage. The thermal system shows better heat retention and quicker recovery, making it more effective for continuous hot water supply.

4.2.2 | Accumulated Hourly Energy Profiles

Figure 6a–c display hourly energy production curves for the PV system and solar thermal system over a week under three typical

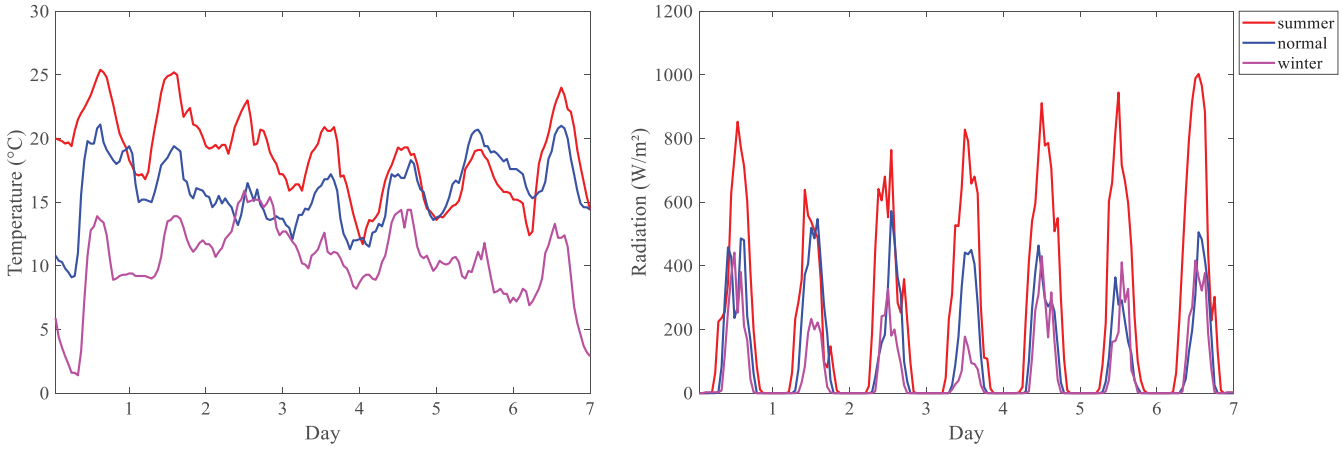

(a) Ambient temperature (b) Solar irradiance

FIGURE 4 | Seven-day weather conditions under three typical weather conditions.

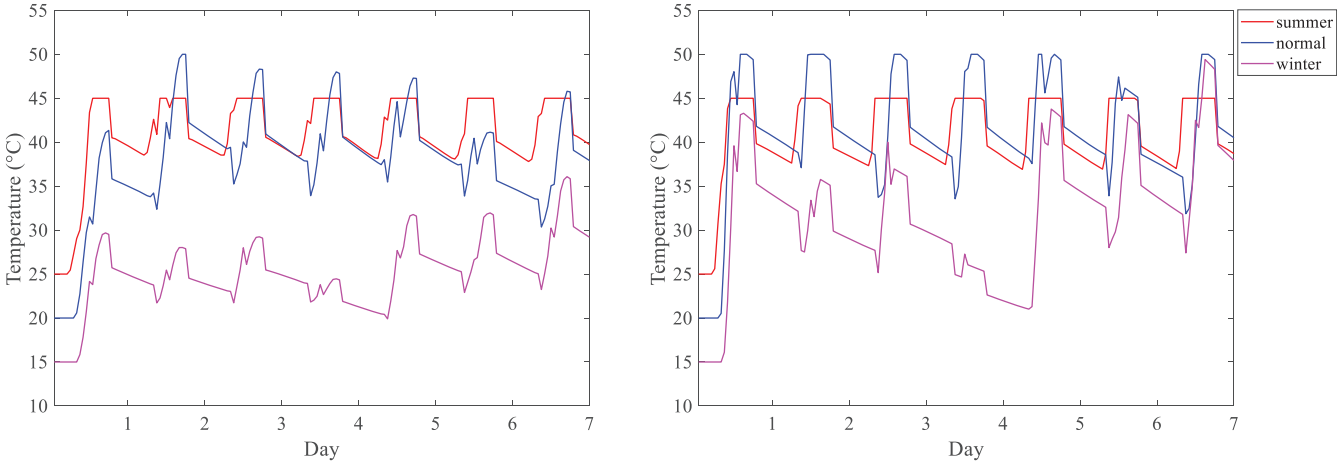

(a) PV system **(b)** Thermal system

FIGURE 5 | Variation of water temperature inside storage tank.

weather conditions. The PV system's energy production profile exhibits its highest output in summer, a smaller and more concentrated range during normal weather conditions, and further reduced levels in winter. The thermal system follows a similar trend but generates significantly higher output compared to the PV system. This difference arises because the solar thermal systems convert absorbed solar radiation directly into heat, enabling more consistent energy delivery during daylight fluctuations. In contrast, PV systems rely on instantaneous photon-electron conversion, making their output more sensitive to transient cloud cover and irradiance variations.

Figures 7a–c and 8a–c display the hourly energy consumption curves of the solar-PV and solar-thermal systems, respectively, over a week under the same three typical climatic conditions. The overall energy consumption patterns show distinct water usage trends, with peaks that vary based on temperature and solar radiation. Taking summer as an example, both PV system (Figure 7a) and thermal system (Figure 8a) exhibit pronounced consumption peaks at 09:00 and 13:00, directly linked to recovery heating demand following water-draw events. Notably, the evening peak at 19:00 in PV systems shows reduced amount compared to the morning peaks, primarily due to constrained thermal recovery under lower ambient temperatures and reduced solar irradiance. The solar-thermal systems demonstrate a more pronounced evening peak than PV systems. This difference stems from their core function: thermal systems directly heat and store hot water, sustaining higher demand for reheating after evening draws. PV systems only produce electricity and don't store heat, so they fully rely on backup electric heaters to recover energy. This method is less efficient when sunlight decreases.

4.2.3 | Accumulated Daily Energy Profiles

Figure 9a,b show the daily energy consumption curves of the solar-PV system and the solar-thermal system over a week under three typical weather conditions. The PV system exhibits average daily energy consumption of 2.85 kWh in summer, 1.47 kWh under normal weather conditions, and 0.86 kWh in winter. In comparison, the solar thermal system demonstrates higher daily energy consumption, with daily averages of 3.04, 2.46, and 1.27 kWh for summer, normal weather, and winter

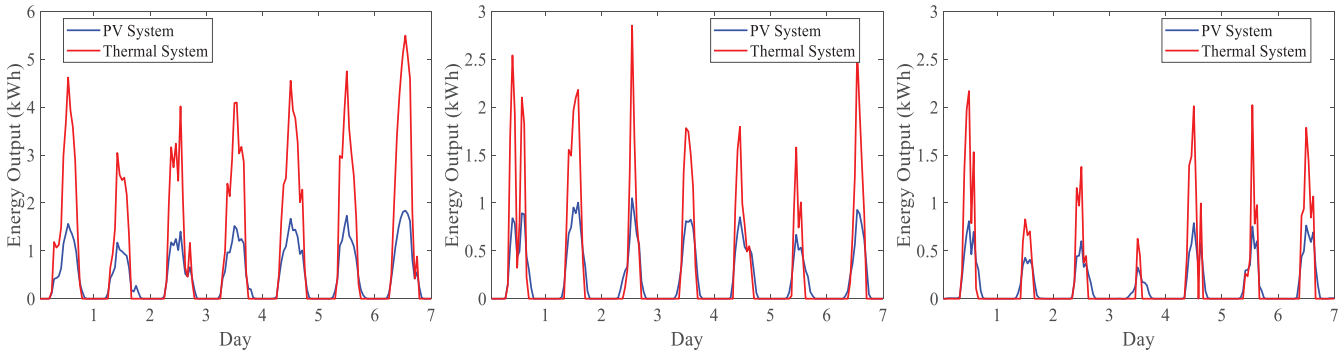

FIGURE 6 | Hourly energy production for two systems over a week under three typical weather conditions.

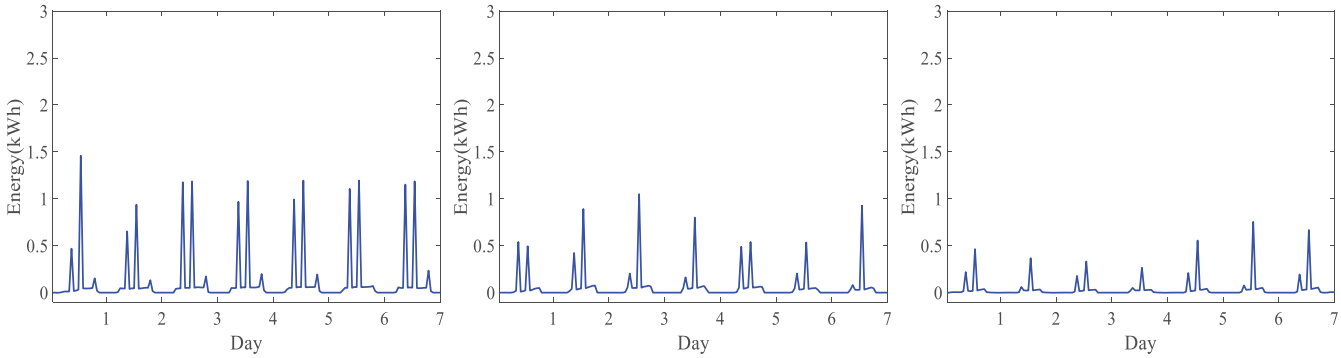

FIGURE 7 | Hourly energy consumption patterns of the solar-PV system over a week under three typical climatic conditions.

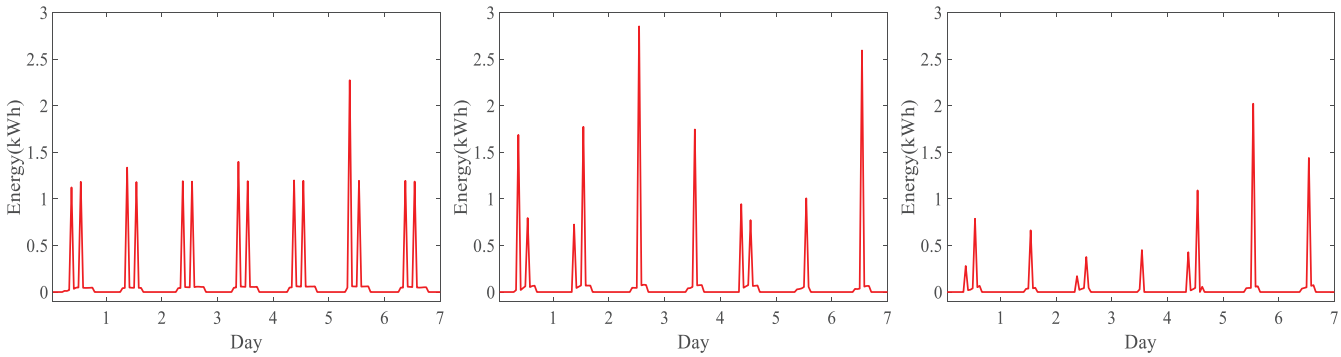

FIGURE 8 | Hourly energy consumption patterns of the solar-thermal system over a week under three typical climatic conditions.

conditions, respectively. Both systems exhibit pronounced consumption peaks at 09:00 and 13:00, directly linked to recovery heating demand following water-draw events. Notably, the evening peak at 19:00 in PV systems shows reduced amount compared to the morning peaks, primarily due to constrained thermal recovery under lower ambient temperatures and diminished solar irradiance.

Figure 10a,b display daily energy production of the PV system and thermal system over a week under three typical climatic conditions. The PV system exhibits average daily energy outputs of 11.52 kWh in summer, 5.15 kWh under transitional weather conditions, and 3.16 kWh during winter. In comparison, the solar thermal system demonstrates significantly higher daily outputs of 27.07, 8.58, and 5.13 kWh for summer, normal weather, and winter conditions, respectively. The solar thermal system consistently outperforms the PV system across all three seasons, though both exhibit substantial seasonal variability. These results highlight the thermal system's superior energy conversion efficiency, particularly pronounced under peak solar irradiation like summer. However, thermal performance shows greater sensitivity to seasonal shifts compared to PV technology. The thermal system's

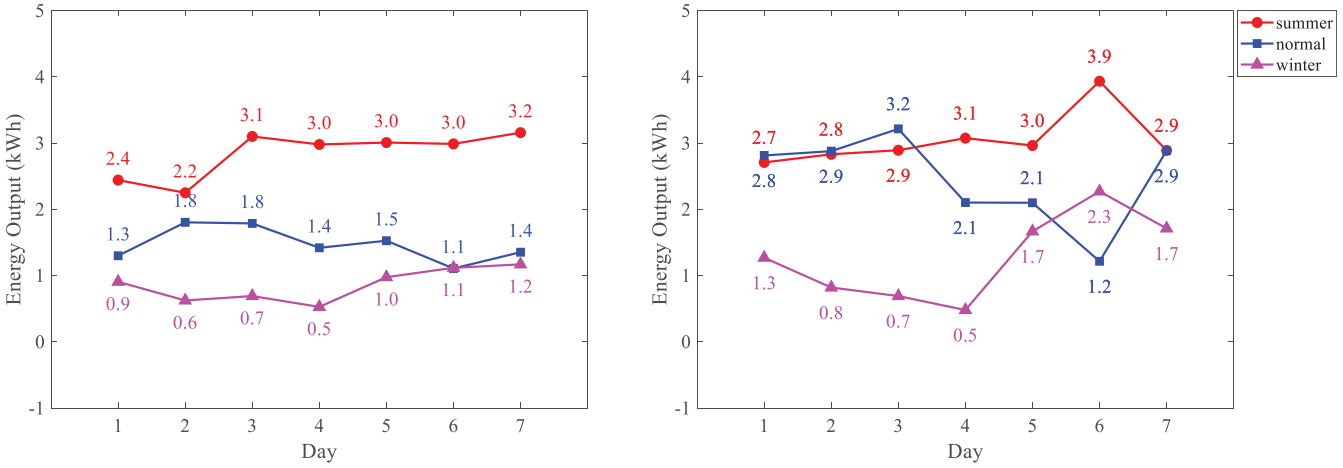

(a) PV system (b) Thermal system

FIGURE 9 | Daily energy consumption patterns for two systems.

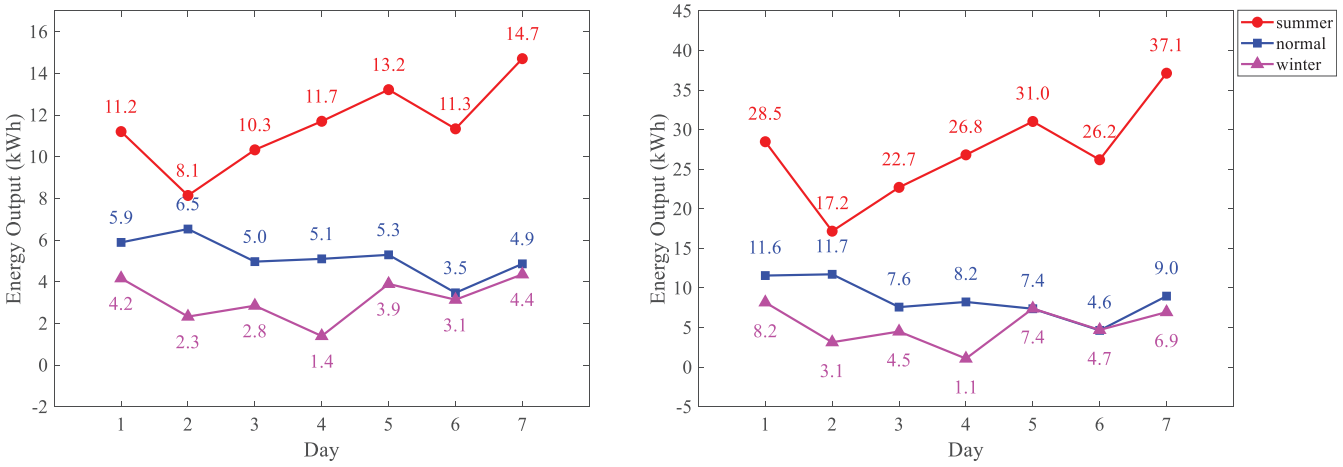

(a) PV system (b) Thermal system

FIGURE 10 | Daily energy production for two systems.

seasonal sensitivity arises from its direct dependence on solar thermal gain and ambient temperature differences. Strong summer sunlight and high temperatures enhance heat absorption and reduce losses, whereas cold winter conditions increase heat loss.

4.2.4 | Accumulated Weekly Energy Profiles

Figure 11a,b present the seven-day accumulated energy consumption for the solar-PV and solar-thermal systems, respectively, under three typical weather conditions. The cumulative energy consumption data reveal that the solar thermal system outperforms the PV system in all seasons. Specifically, the PV system's energy consumption in summer, transitional weather, and winter is 19.9, 10.3, and 6.3 kWh, respectively, while the solar thermal system consumes 21.3, 17.2, and 8.9 kWh during the same periods, which represent performance advantages of 7.0%, 67.0%, and 62.4% over the PV system. Notably, under summer conditions with high temperatures and rich solar radiation, the solar thermal system exhibits only 1.4 kWh higher energy consumption than the solar PV system, equating to a 7.0% performance advantage.

Figure 12a,b present the seven-day cumulative energy production for the solar-PV and solar-thermal systems, respectively, under three typical weather conditions. The PV system exhibits pronounced seasonal fluctuations: summer production exceeds normal weather output by 123.3% and winter output by 264.7%, while normal weather production is 63.3% higher than winter. In contrast, the solar thermal system demonstrates even more significant seasonal variations. Its summer output surpasses transitional weather and winter levels by 215.3% and 427.9%, respectively, while transitional weather production remains 67.4% higher than winter. These findings reveal that while both systems peak in summer, the solar thermal system exhibits greater seasonal amount. The difference between summer and winter performance is significantly greater in the solar thermal system (427.9%) than in the PV system (264.7%), highlighting the thermal system's stronger sensitivity to seasonal changes.

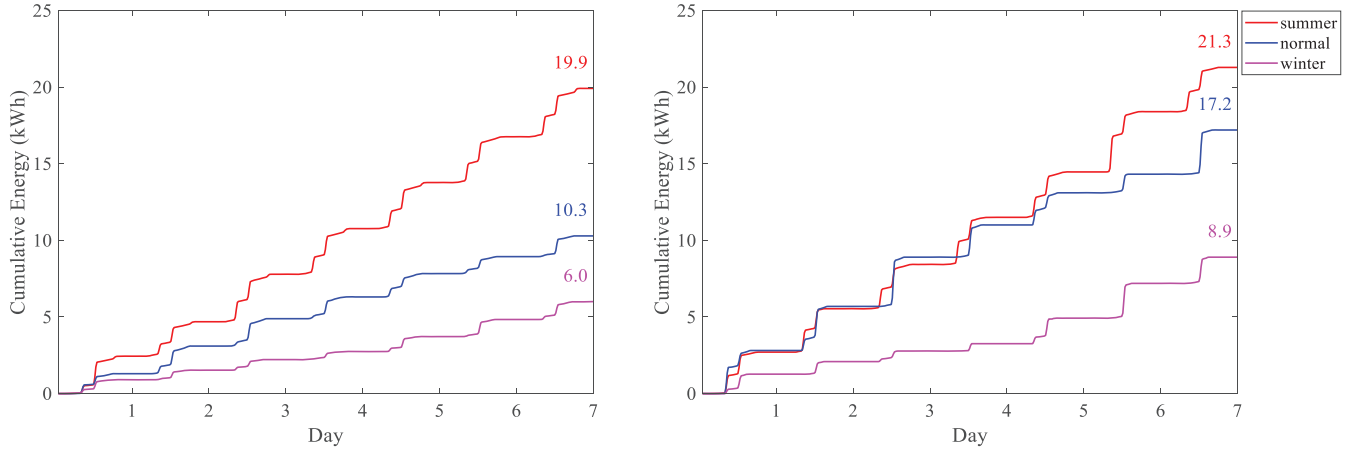

FIGURE 11 | Weekly energy consumption curves over a week for two systems.

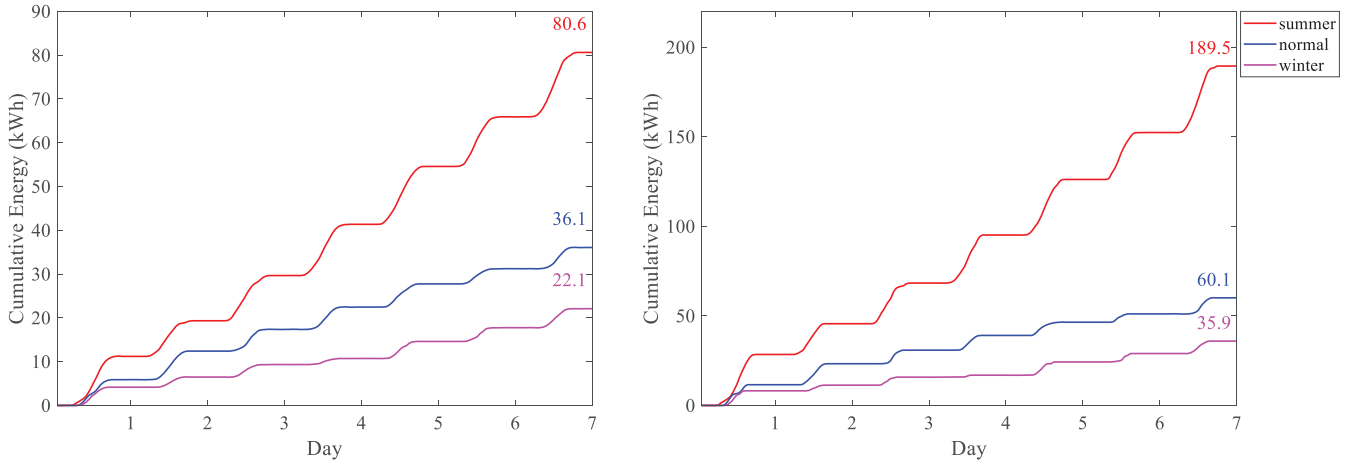

FIGURE 12 | Weekly energy production curves over a week for two systems.

4.2.5 | System Efficiency and Economic Analysis

Figure 13a–c, respectively, display the hourly COP curves of solar-thermal and solar-PV systems over 1 week under three typical climatic conditions. In summer, the performance of the solar thermal system is limited by the target water temperature of 45°C. Since this temperature is easily reached, not all available solar energy is utilized. As a result, the system appears less efficient during peak summer. In contrast, during normal and winter weather, more of the solar energy is used for heating, leading to higher peak COP values. However, the thermal system is highly dependent on both solar radiation and ambient temperature, causing its COP to fluctuate noticeably with changing weather. Meanwhile, the PV system remains much more stable, consistently delivering a COP between 0 and 0.2 with the variation of weather conditions.

Figure 14a,b present the total annual amount of energy consumption and the energy production for the solar-PV and solar-thermal systems, respectively. Based on New Zealand's climatic characteristics (Southern Hemisphere), the seasonal division is as follows: Summer spans December to February, winter occurs from June to August, and the remaining months (March–May and September–November) constitute transitional seasons. Under Auckland's climatic conditions, the solar PV system consumes 721.38 kWh annually, while the solar thermal system consumes 964.59 kWh of thermal energy. This represents 33.7% higher thermal system consumption (with the difference of 243.21 kWh), enabling stable water supply per equivalent 10 m^2 area. The solar PV system produces 2780.41 kWh annually, while the solar thermal system produces 5847.59 kWh of thermal energy. This reflects 110.3% higher thermal system production (with the difference of 3067.18 kWh), demonstrating superior energy yield per equivalent 10 m^2 area. The thermal system's significantly higher production surplus highlights its thermodynamic strength, since it converts solar energy directly into heat, reducing energy loss compared to the PV system, which converts electricity into heat.

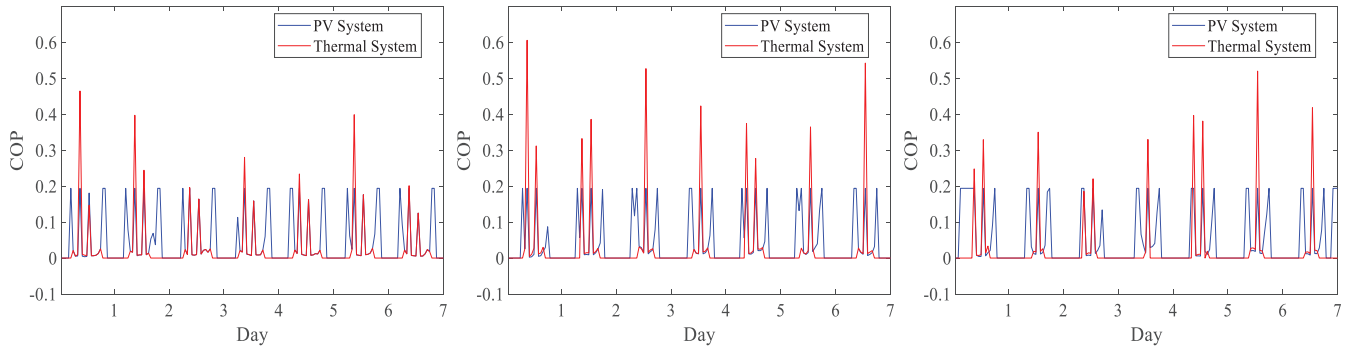

FIGURE 13 | Hourly COP curves over a week for two systems under three typical climatic conditions.

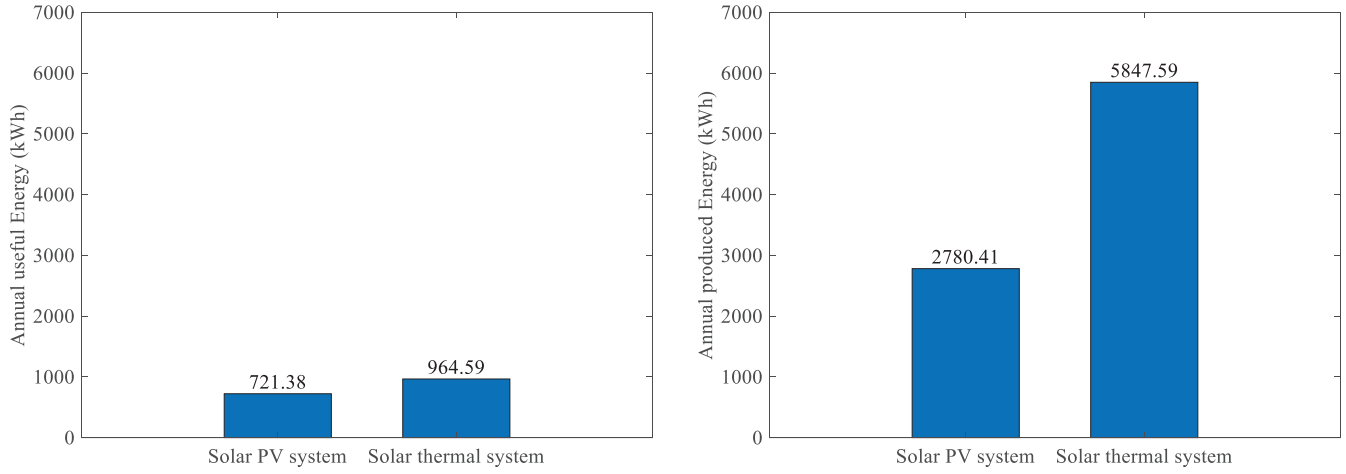

FIGURE 14 | Annual energy profiles for both systems.

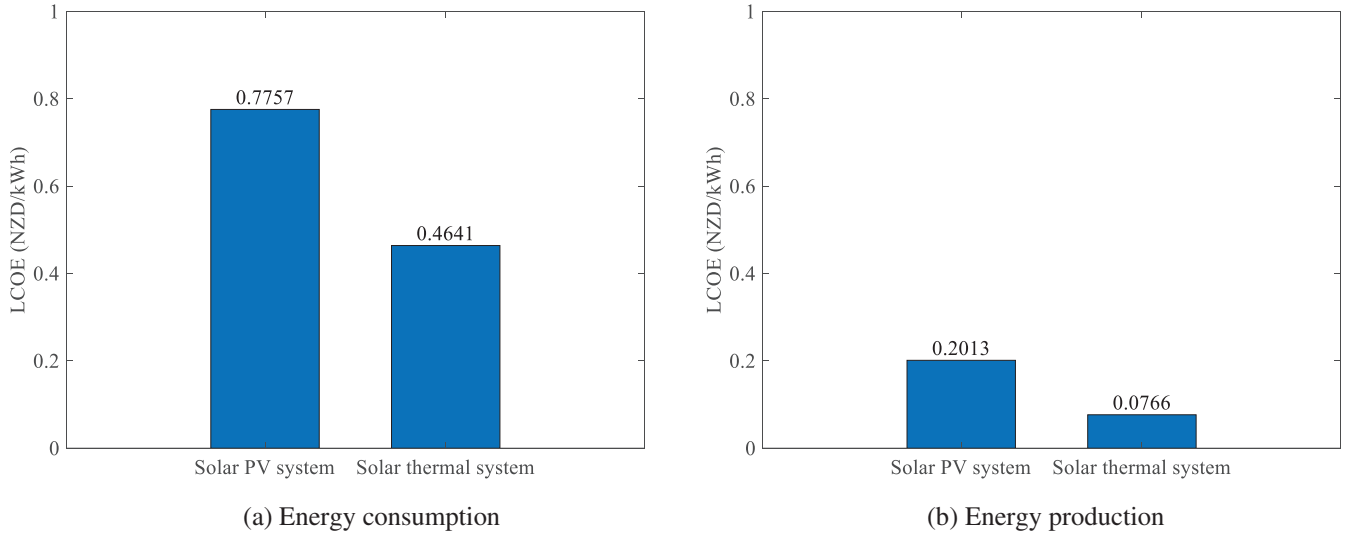

FIGURE 15 | LCOE for both systems.

Figure 15a,b present the LCOE of the energy consumption and the energy production for the solar-PV and solar-thermal systems, respectively. With a 25-year lifespan, the solar thermal system costs 7500 NZD, while the PV system costs 6000 NZD. Using a 5% discount rate, annual operating costs at 1% of the investment, and a 5% decommissioning value, the thermal system proves far more economical. Its cost per unit of energy consumption (LCOE) is 0.4641 NZD/kWh, which is 40.2% lower than the PV system's 0.7757 NZD/kWh, saving 0.3116 NZD per kWh. For energy production, the thermal system's LCOE is 0.0766 NZD/kWh, just 38.1% of the PV system's 0.2013 NZD/kWh, cutting costs by 61.9%.

The efficiency difference grows over time, as thermal systems harvest sunlight more effectively during Auckland's mild winters and transitional seasons. Unlike PV systems, which require an extra conversion step to produce heat, solar thermal collectors transfer heat directly, reducing energy losses. While PV offers flexible electricity for various household uses, thermal systems are far more efficient for direct water heating. Additionally, thermal output often better matches typical hot water demand times, improving overall system effectiveness.

Based on the research findings, under real-world climate and household water usage scenarios, solar thermal systems demonstrate advantages over PV systems in both energy efficiency and full-life-cycle economics: the annual energy output of solar thermal is 110.3% higher, and its LCOE is 61.9% lower, making it a superior engineering choice for domestic hot water applications. However, the output of solar thermal systems exhibits stronger seasonal fluctuations (summer output is 4.3 times that of winter), and its performance coefficient is notably influenced by weather conditions. Therefore, system design must prioritize optimizing winter performance and configuring auxiliary energy support. In contrast, although PV system output also declines seasonally, its operation remains more stable overall. The modeling approach developed in this study, which integrates real climate data and water usage patterns, provides a reliable basis for accurately predicting system performance and optimizing configuration in practical engineering applications.

5 | Conclusion

This study has systematically investigated the accumulated performance of the solar-PV and solar-thermal water heaters across consecutive operational cycles under real New Zealand's typical weather conditions. This study employs a streamlined system modeling approach integrated with the NIWA climate data to address key challenges in predicting the accumulated system performance. Several conclusions can be drawn from this study:

1. The highlight of the study is that the water performance within the storage tank has been investigated under real-life operating conditions, which consider the impact of actual weather fluctuations (including ambient temperature, solar radiation, and sunshine hours), target hot water temperature, heat losses from the tank, and typical household water usage patterns along with the replenishment of cold water.
2. Based on the numerical analysis, the solar thermal system outperforms the solar PV system in annual and daily energy production and energy consumption. The solar thermal system generated 5847.59 kWh/year per 10 m^2 collector area, which is 110.3% higher than the PV system's 2780.41 kWh/year, while consuming 33.7% more auxiliary energy annually at 964.59 kWh versus the PV system's 721.38 kWh.
3. Both systems show seasonal fluctuations, but the solar thermal system exhibits greater amplitude. The thermal system output in summer was 427.9% higher than in winter, while PV output was 264.7% higher. For the thermal system, daily energy use fell from 3.04 kWh in summer to 1.27 kWh in winter. PV had a steeper decline, dropping from 2.85 kWh to just 0.86 kWh.
4. In summer, the COP of solar thermal system is limited by the target water temperature of 45°C. In contrast, more of the solar energy is used for heating during normal and winter weather, leading to higher peak COP values. The solar thermal system is highly dependent on the weather, causing its COP to fluctuate noticeably, while the PV system remains more stable, consistently delivering a COP between 0 and 0.2 with the variation of weather.
5. The solar thermal system is more cost-effective than the PV system over a lifespan of 25-year period, with 40.2% lower LCOE for energy consumption and 61.9% lower for energy production. Compared to the solar-PV system (which requires an extra conversion step to produce heat), solar thermal collectors transfer heat directly, reducing energy losses.

Future studies will focus on the integration of energy and thermal storage into the current solar-PV and solar-thermal systems, respectively, in order to evaluate and compare the accumulated performance under real weather conditions.

Nomenclature

a	time (h)
A	panel area (m^2)
A_c	solar collector area (m^2)
A_{tank}	surface area of tank (m^2)
C_b	bond conductance (W/m·K)
C_p	specific heat (J/kg·K)
D	tube diameter (m)
D_i	Inner diameter of tube (m)
D_t	decommissioning value (NZD)
f	friction factor
F	standard fin efficiency
F'	collector efficiency factor
F_r	collector heat removal factor
G	solar irradiance on a horizontal surface (W/m^2)
G_t	solar irradiance on a tilted surface (W/m^2)
h_{fi}	the heat transfer coefficient (W/m^2K)
i	hour index

I_t investment cost (NZD)

k thermal conductivity of fluid (W/m·K)

k_{plate} thermal conductivity of plate (W/m·K)

m the fin parameter (m^{-1})

$\dot{m}$ mass flow rate (kg/s)

m_{use} amount of water mass used (kg)

M water mass in the tank (kg)

Nu nusselt number

O_t operational costs (NZD)

Pr prandtl number

q_i hourly energy input (J)

Q_{all} total solar energy (J)

Q_{eff} total usable thermal energy delivered to water heating (J)

Q_{loss} energy loss in the tank (J)

Q_{out} daily net PV power output (J)

Q_u useful energy gain (J)

Re Reynolds number

S rated annual energy output (J)

u dynamic viscosity (Pa·s)

U_L overall heat loss coefficient (W/m^2K)

U_{tank} heat loss coefficient of tank (W/m^2K)

V_{tank} total water volume in the tank (L)

W distance between the tubes (m)

r country-specific discount rate

t year index

T project lifetime (yrs)

T_a ambient air temperature (°C)

T_{cold} cold water temperature in the tank (°C)

T_f final temperature (°C)

$T_{f,i-1}$ final water temperature at an hour $i-1$ (°C)

T_i inlet water temperature (°C)

T_{max} max water temperature (°C)

T_{PV} PV temperature (°C)

T_{use} water temperature after usage (°C)

Greek letters

μ fluid speed (Pa·s)

τ_α transmittance-absorptance

θ tilt angle (°)

ρ density (kg/m^3)

η_{inv} inverter efficiency

η_{PV} PV system efficiency

δ absorber plate thickness (m)

Author Contributions

Wei Lu: methodology, software, data curation, investigation, writing – original draft, visualization, formal analysis. **Jay Wang:** conceptualization, methodology, supervision, investigation, writing – review and editing.

Acknowledgments

The authors have nothing to report.

Conflicts of Interest

The authors declare no conflicts of interest.

Data Availability Statement

The data that support the findings of this study are available from the corresponding author upon reasonable request.

References

1. T. Harlan and J. Baka, "Stacked Energyscapes: Conceptualizing Fossil Fuel and Renewable Energy Entanglements in Low-Carbon Transitions," *Energy Research & Social Science* 115 (2024): 103648.

2. B. Kamana-Williams and D. Bishop, "Flexible Futures: The Potential for Electrical Energy Demand Response in New Zealand," *Energy Policy* 195 (2024): 114387.

3. A. Marcos-Castro, C. Sanz-Saiz, J. Polo, and N. Martín-Chivelet, "Performance Ratio Estimation for Building-Integrated Photovoltaics—Thermal and Angular Characterisation," *Applied Sciences* 15, no. 12 (2025): 6579.

4. J. Wang, E. Hu, A. Blazewicz, and A. W. Ezzat, "Simulation of Accumulated Performance of a Solar Thermal Powered Adsorption Refrigeration System With Daily Climate Conditions," *Energy* 165 (2018): 487–498.

5. J. Wang, E. Hu, A. Blazewicz, and A. W. Ezzat, "Investigation on the Long-Term Performance of Solar Thermal Powered Adsorption Refrigeration System Based on Hourly Accumulated Daily Cycles," *Heat and Mass Transfer* 57, no. 2 (2021): 361–375.

6. Z. Xiao, Y. Chen, D. Wang, et al., "Performance Analysis of Photovoltaic Residual Electricity Thermal Conversion and Storage System in Solar Energy Enrichment Areas," *Solar Energy* 274 (2024): 112562.

7. S. Thakur, D. Singh, U. N. Mughal, V. Kumar, and R. K. Calay, "Comparative Life Cycle Assessment of Solar Thermal, Solar PV, and Biogas Energy Systems: Insights From Case Studies," *Applied Sciences* 15, no. 14 (2025): 8082.

8. T. H. Snelder, J. R. Leathwick, K. L. Dey, et al., "Development of an Ecologic Marine Classification in the New Zealand Region," *Environmental Management* 39 (2007): 12–29.

9. H. Liu, Z. Huang, K. Liu, X. Hu, and J. Zhou, "Interfacial Solar-to-Heat Conversion for Desalination," *Advanced Energy Materials* 9, no. 21 (2019): 1900310.

10. M. Herrando and A. Ramos, "Photovoltaic-Thermal (PV-T) Systems for Combined Cooling, Heating and Power in Buildings: A Review," *Energies* 15, no. 9 (2022): 3021.

11. E. Halawa, K. C. Chang, and M. Yoshinaga, "Thermal Performance Evaluation of Solar Water Heating Systems in Australia, Taiwan and Japan – A Comparative Review," *Renewable Energy* 83 (2015): 1279–1286.

12. W. Xu, H. Guo, and C. Ma, "An Active Solar Water Wall for Passive Solar Greenhouse Heating," *Applied Energy* 308 (2022): 118270.

13. D. Bishop, T. Nankivell, and B. Williams, "Peak Loads vs. Cold Showers: The Impact of Existing and Emerging Hot Water Controllers on Load Management," *Journal of the Royal Society of New Zealand* 55, no. 4 (2025): 1111–1136.

14. M. E. Zayed, S. Rehman, I. A. Elgendy, et al., "Benchmarking Reinforcement Learning and Prototyping Development of Floating Solar Power System: Experimental Study and LSTM Modeling Combined With Brown-Bear Optimization Algorithm," *Energy Conversion and Management* 332 (2025): 119696.

15. B. Shboul, M. E. Zayed, W. M. Ashraf, et al., "Energy and Economic Analysis of Building Integrated Photovoltaic Thermal System: Seasonal Dynamic Modeling Assisted With Machine Learning-Aided Method and Multi-Objective Genetic Optimization," *Alexandria Engineering Journal* 94 (2024): 131–148.

16. B. Shboul, M. E. Zayed, A. S. Abdelrazik, M. Alrbai, A. S. Odat, and F. Almomani, "Exergoeconomic and Environmental Impact Assessment of a Semi-Scale Office With Solar Chimney and Evaporative Cooling Tower for Sustainable Space Cooling and Air Ventilation," *Energy Conversion and Management: X* 27 (2025): 101191.

17. Y. Jia, F. Ran, C. Zhu, and G. Fang, "Numerical Analysis of Photovoltaic-Thermal Collector Using Nanofluid as a Coolant," *Solar Energy* 196 (2020): 625–636.

18. V. Gnielinski, "New Equations for Heat and Mass Transfer in the Turbulent Flow in Pipes and Channels," 41 (1975): 8–16.

19. G. K. Filonenko, "Friction Factor for Turbulent Pipe Flow," *Teploenergetika* 1 (1954): 40–44.

20. G. Góngora-Gallardo, M. Castro-Gil, A. Colmenar-Santos, and M. Tawfik, "Efficiency Factors of Solar Collectors of Parallel Plates for Water," *Solar Energy* 94 (2013): 335–343.

21. S. Farahat, F. Sarhaddi, and H. Ajam, "Exergetic Optimization of Flat Plate Solar Collectors," *Renewable Energy* 34, no. 4 (2009): 1169–1174.

22. M. Elnaggar, "Useful Energy, Economic and Reduction of Greenhouse Gas Emissions Assessment of Solar Water Heater and Solar Air Heater for Heating Purposes in Gaza, Palestine," *Heliyon* 9, no. 6 (2023): e16803.

23. G. Notton, V. Lazarov, and L. Stoyanov, "Optimal Sizing of a Grid-Connected PV System for Various PV Module Technologies and Inclinations, Inverter Efficiency Characteristics and Locations," *Renewable Energy* 35, no. 2 (2010): 541–554.

24. E. Skoplaki and J. A. Palyvos, "On the Temperature Dependence of Photovoltaic Module Electrical Performance: A Review of Efficiency/Power Correlations," *Solar Energy* 83, no. 5 (2009): 614–624.

25. H. Mousa, J. Naser, and O. Houche, "Using PCM as Energy Storage Material in Water Tanks: Theoretical and Experimental Investigation," *Journal of Energy Storage* 22 (2019): 1–7.

26. D. Luo, Y. Zhao, J. Cao, W. H. Chen, Y. Zhao, and B. Cao, "Performance Analysis of a Novel Thermoelectric-Based Battery Thermal Management System," *Renewable Energy* 224 (2024): 120193.

27. A. C. Brent, A. Crossland, and D. Ranusa, "An Assessment of the Economic Feasibility of the Floating PV Technology in Aotearoa–New Zealand," *Sustainable Energy Technologies and Assessments* 57 (2023): 103284.

28. "Obtaining Climate Data From NIWA," cited July 20, 2025, https://niwa.co.nz/climate-and-weather/obtaining-climate-data-niwa.